Available online at www.sciencedirect.com
ScienceDirect
Catalysis Today 131 (2008) 393–401
CATALYSIS TODAY
www.elsevier.com/locate/cattod

Effect of method of preparation on the activity and selectivity of iron phosphate catalyst in the ammoxidation of 2-methyl pyrazine

P. Nagaraju [a], Ch. Srilakshmi [b], Nayeem Pasha [a], N. Lingaiah [a], I. Suryanarayana [a], P.S. Sai Prasad [a,*]

[a] *Inorganic & Physical Chemistry Division, Indian Institute of Chemical Technology, Hyderabad 500007, India*
[b] *Institute of Chemical and Engineering Sciences (ICES), 1 Pesek Road, Jurong Island, Singapore 627833*

Available online 16 January 2008

Abstract

Ammoxidation of methylpyrazine (MP) to cyanopyrazine (CP) was performed at 633–693 K over iron phosphate catalysts having a P/Fe ratio of 1.2, obtained by adopting different methods of catalyst preparation. The catalysts were characterized by XRD, FTIR, UV-DRS, laser-Raman spectroscopy, TPR, TEM, XPS, acidity by Potentiometric titration and TPD of NH_3. XRD and Raman data suggested predominant formation of quartz phase of iron phosphate. The structure and texture of the catalysts varied with the nature of starting material as well as the preparation method. The catalytic activity depended on the extent of quartz phase formation. Precipitation in the basic medium improved quartz phase formation and enhanced the activity. However, the decreased acid strength caused reduction in nitrile selectivity. A judicious combination of the redox and acid strength properties is required for obtaining maximum yield of CP.

Keywords: Iron phosphate; Ammoxidation; 2-Methyl pyrazine; 2-Cyano pyrazine

1. Introduction

The heterogeneously catalyzed vapor phase ammoxidation of alkyl aromatics and hetero alkyl aromatics to their corresponding nitriles is an industrially important reaction. The products are valuable intermediates in the synthesis of several dyestuffs, pesticides and pharmaceuticals [1]. Amidopyrazine, often referred to as pyrazinamide, is an important anti-tubercular drug. It is conventionally prepared by a non-catalytic multi-step process which is economically as well as environmentally disadvantageous [2]. Vapor phase processes are advantageous compared to liquid phase reactions in terms of continuous processing, easy catalyst handling, homogeneity of the reaction mixture and environmental acceptability [3]. Ammoxidation refers to the interaction of ammonia with reducible organic material (alkyl aromatics or heteroalkyl aromatics, Scheme 1) in the presence of oxygen [4]. For this reaction the catalyst should possess both acidic and redox functionalities [5]. Even though, iron phosphate possesses both acidic and redox properties as molybdenum and vanadium phosphates, it has received less attention [6,7] for ammoxidation. Very few references exist on its characterization and catalytic application. An adsorption–desorption study by Gadgil and Kulshreshtha [8] reveals that both Bronsted and Lewis acid sites are present in $FePO_4$ catalyst. Ai et al. [9–12] have reported the effects of method of preparation of iron phosphate catalyst and its unique catalytic performance at a P/Fe atomic ratio of 1.15–1.2 for oxidative dehydrogenation reactions.

As a part of our on going study on ammoxidation of methylpyrazine (MP), we have recently reported [13] the activity and selectivity functionalities of iron phosphate prepared with different P/Fe atomic ratios ranging from 1 to 1.6, and revealed that the $FePO_4$ with a P/Fe atomic ratio of 1.2 offers highest selectivity towards cyanopyrazine (CP) (98%). The aim of the present study is to explore a suitable method of preparation by means of which the conversion could be enhanced, still retaining the superior selectivity. Iron phosphate catalysts with a fixed P/Fe atomic ratio of 1.2, prepared by different methods have been examined in order to establish the structure-activity relationship.

* Corresponding author. Tel.: +91 40 2719 3163; fax: +91 40 27160921.
E-mail address: saiprasad@iict.res.in (P.S. Sai Prasad).

0920-5861/$ – see front matter © 2008 Published by Elsevier B.V.
doi:10.1016/j.cattod.2007.10.057

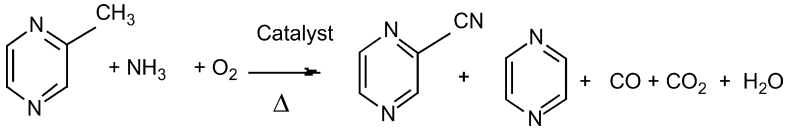

Scheme 1.

2. Experimental

2.1. Preparation of catalysts

Iron phosphate catalysts, with a constant P/Fe atomic ratio of 1.2, were prepared by the following methods:

2.1.1. Method A

$Fe(NO_3)_3{}^{\bullet}9H_2O$ was dissolved in water and dilute urea solution was added to precipitate iron hydroxide gel. The precipitate was filtered and the gel was mixed with desired amount of 85% H_3PO_4. The mixture was boiled slowly for 1–2 h and then the excess water was evaporated to yield a paste.

2.1.2. Method B

In this method $FePO_4$ was synthesized from a mixture of $Fe(NO_3)_3{}^{\bullet}9H_2O$ and $NH_4H_2PO_4$. Aqueous solutions of iron nitrate and ammonium dihydrogen phosphate, in appropriate quantities were mixed and the solution was evaporated at 363 K.

2.1.3. Method C

Appropriate quantities of $Fe(NO_3)_3{}^{\bullet}9H_2O$ and 85% H_3PO_4 were mixed in water and the excess water was subsequently evaporated.

2.1.4. Method D

The preparation was similar to Method B. However, $(NH_4)_2HPO_4$ was used instead of $NH_4H_2PO_4$.

2.1.5. Method E

In this method ammonia was used instead of urea for the precipitation and the rest of the procedure was the same as in Method A. The catalyst masses were subjected to air-drying at 393 K for 12 h before calcination in air at 823 K for 4 h. The finished catalysts were named correspondingly as catalysts A, B, C, D and E based on the method of preparation.

The Fe concentration in the catalysts, as determined by the AAS analysis, agreed well with that of the amount of iron taken in the solution for preparation. (295 mg/l in the solution vs. 286 ± 5 mg/l of the finished catalysts.)

2.2. Characterization of fresh catalysts

BET surface areas of the catalysts were determined on a Micromeritics (Auto Chem-2910) instrument with nitrogen physisorption at 77 K, taking 0.169 nm^2 as the cross sectional area of dinitrogen. XRD patterns of the catalysts were obtained with a Rigaku Miniflex diffractometer, using Cu Kα radiation (1.5405 Å) at 30 kV and 150 mA.The average crystallite size was determined from the XRD patterns using the Scherrer equation [14]. The extent of quartz phase formation, as represented by the area of the peak at $2\theta = 25.8$ Å in the X-ray difractogram, was calculated as reported by Nagaraju et al. [13]. FTIR spectra were recorded on a DIGILAB (USA) spectrometer, with a resolution of 1 cm^{-1} using KBr disc method. The iron content was determined by atomic absorption spectroscopy using a Perkin–Elmer Analyst 300 double beam spectrometer. The powders were first dissolved in acidic solution (aquaregia) and diluted to concentrations within the detection range of the instrument.

Diffuse reflectance spectra of the catalysts samples were recorded in the UV–vis region (200–800 nm) with GBC Cintra 10_e spectrometer with a slit width of 1.5 nm and a scan speed of 400 nm/min. The Raman spectra of the samples were collected on a UV–vis Raman spectrometer system (Horiba-Jobin Yvon LabRam-HR) equipped with a confocal microscope, 2400/900 grooves/mm gratings, and a notch filter.

Transmission electron microscope (TEM) photographs were obtained using Tecnai-12 FEI instrument operating at 120 kV. Temperature programmed reduction (TPR) of the catalysts was carried out in a flow of 10% H_2/Ar mixture gas at a flow rate of 30 ml/min with a temperature ramp of 10 K/min. Before the TPR run the catalysts were pretreated with Ar at 523 K for 2 h. The hydrogen consumption was monitored using a thermal conductivity detector.

XPS measurements of the catalysts were conducted on a Kratos axis 165 apparatus equipped with a dual anode (Mg and Al) using the Mg Kα source. The carbon 1s binding energy of 284.6 eV was used as a reference for determining the binding energies.

The acid strength of the solid samples was measured by the potentiometric titration method [15,16]. Temperature programmed desorption of ammonia (TPD) was performed using 100 mg of catalyst after pretreatment at 573 K under a dry He flow (50 cm^3/min). The catalyst was exposed to NH_3 from a gas mixture containing 10% NH_3 in He for 45 min at 373 K and the excess NH_3 was removed under a He flow (50 cm^3/min). The temperature of the sample was raised at a rate of 10 K/min up to 1073 K, and the desorbed gas was monitored by using a gas chromatograph with a TCD detector.

2.3. Catalytic reaction

The ammoxidation was carried out in a fixed-bed flow reactor under vapor phase at atmospheric pressure in the temperature range of 633–693 K, with a molar ratio of MP:water:ammonia:air = 1:13:17:38 using 3 g of catalyst and an MP flow rate of 2 ml/h. The detailed procedure is available elsewhere [13].

Table 1
The physico–chemical characteristics of the catalysts

Method of preparation	Surface area (m^2/g)	Acid strength E (mV)	TPD of NH_3 (μm/g) desorbed	Selectivity (%) to CP at 673 K	Crystallite size from XRD (nm)	Average particle size TEM (nm)
A	1.3	530	1580	94.0	27.3	40
B	3.8	440	983	98.0	19.2	45
C	27.0	390	735	77.0	19.4	45
D	3.9	330	640	70.0	18.1	42
E	32.0	288	586	66.5	37.2	50

3. Results and discussion

3.1. BET surface area of the catalysts

The surface areas of the samples are summarized in Table 1. The surface area of the catalysts varied with method of preparation and precursor used. Among all the catalysts, catalyst E showed a high surface area of 32 m^2/g. The lowest value was exhibited by catalyst A in which urea solution was used as the precipitating agent.

3.2. X-ray diffraction studies

Fig. 1 shows the powder X-ray diffraction patterns for the $FePO_4$ catalysts. The catalysts were composed of mainly quartz-like phase ($2\theta = 20.2^\circ, 25.8^\circ$) with a small amount of the tridymite phase represented by peaks appearing at 20.2°, 20.95°. The trydimite phase, normally seen up to a calcination temperature of 723 K, is transformed to quartz phase at 823 K. Such a result was also reported by Wang et al. [17]. In the case of catalyst A an amorphous phase appeared up to 673 K and on further heating it was transformed in to quartz phase and a new phase with peaks at 2θ values of 24.5°, 25.0°, 27.0°, 29.8°, 32.5°, 37.9°. Ai and Ohdan [11] designated this phase as M-phase, mainly characterized by three clear peaks at $2\theta = 24.5^\circ$, 32.5°, 37.9°. Interestingly a significant change in relative intensities with respect to quartz phase was observed in all these catalysts. The values for the average crystallite size of these catalysts, calculated using Scherrer equation, are shown in Table 1. The maximum value for the average crystallite size was shown by catalyst E. Thus, the XRD results revealed that the structure of the catalyst depends upon the method of preparation, precursor and calcination temperature.

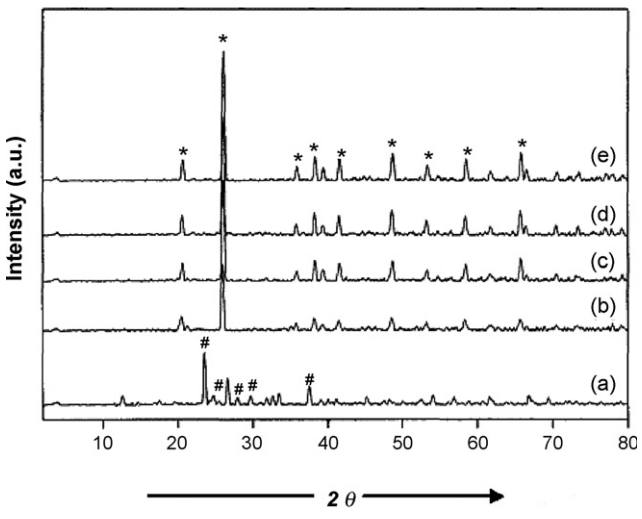

Fig. 1. XRD patterns of (a) catalyst A, (b) catalyst B, (c) catalyst C, (d) catalyst D and (e) catalyst E. (*) Corresponds to FePO4 (Q); (#) corresponds to M-phase.

3.3. Fourier transform infrared spectroscopy studies

Fig. 2 shows the FTIR spectra of the $FePO_4$ samples. All the catalysts showed a very broad band at 3400 cm^{-1} corresponding to surface hydroxyl groups. The band at 1610 cm^{-1} is due to bending vibrational mode of water molecules. It is well known that the peaks in the region between 1200 cm^{-1} and 500 cm^{-1} correspond to the symmetric and asymmetric vibrations of the phosphate groups. The spectra of all the catalysts exhibited a broad band at 1067 cm^{-1} due to asymmetric stretching mode of P═O of the PO_4 group and a band at 510 cm^{-1} due to the bending vibrational mode of phosphate ion [18]. Catalyst A showed shoulder bands at 995 cm^{-1} and 1185 cm^{-1} presumably due to the stretching vibrations resulting from unknown M-phase formed. The results obtained from FTIR spectroscopy confirm the existence of $FePO_4$ formation.

3.4. UV-DRS studies

Fig. 3 shows the UV-DRS spectra of the $FePO_4$ catalysts. The spectra showed a broad absorption band in the range of 200–400 nm with multiplicity. The band at 230 nm could be assigned to the P–O charge transfer transition and the bands at 320 nm and 380 nm to the Fe–O charge transfer transitions [19,20]. In the case of catalyst A, there is a conspicuous decrease in the intensity of the peaks due to quartz phase formation.

3.5. Laser-Raman studies

Fig. 4 shows the UV Raman spectra of the $FePO_4$ catalysts. These catalysts exhibited two intense Raman bands at 1010 cm^{-1} and 1053 cm^{-1} along with weak bands at 408 cm^{-1}, 440 cm^{-1}, 596 cm^{-1}, 665 cm^{-1} and 1167 cm^{-1}. It is known that the stretching and bending vibrations of phosphate groups occur at 1000–1200 cm^{-1} and 400–700 cm^{-1}, respectively. Tetrahedrally coordinated iron gives the Raman bands in the same region when a UV laser of 325 nm is used. Raman bands at 1010 cm^{-1} and 1053 cm^{-1} can be attributed to alternatively connected tetrahedral FeO_4 and PO_4 groups, respectively [21]. The bands at 1167 cm^{-1} and 665 cm^{-1} can be ascribed to the presence of

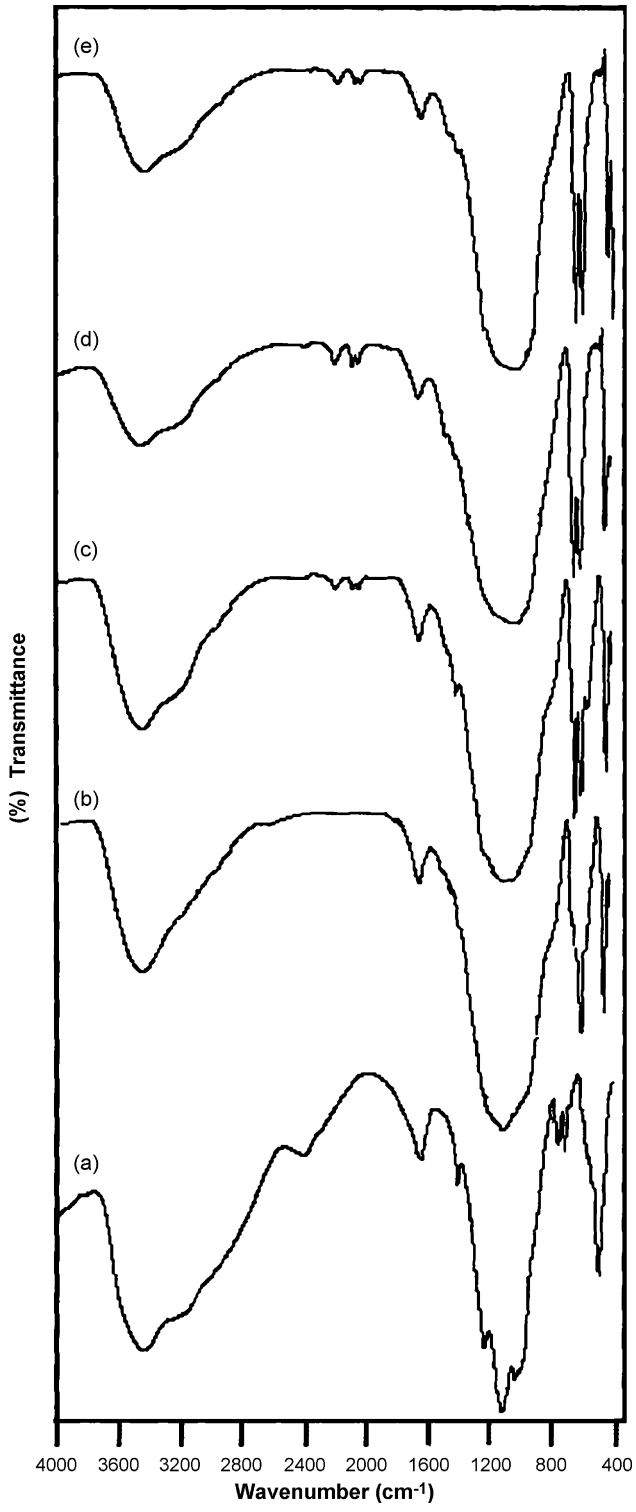

Fig. 2. FTIR spectra of (a) catalyst A, (b) catalyst B, (c) catalyst C, (d) catalyst D and (e) catalyst E.

metaphosphate groups. The catalyst A exhibited new bands at 510 cm^{-1} and 1200 cm^{-1}. These peaks are attributed to the bridging (P–O–P) symmetrical stretching vibration and non-bridging $(PO_2)^-$ symmetrical stretching vibration of the phosphate tetrahedra. Whereas catalysts B to E exhibit a clear chain structure of alternating FeO_4 and PO_4 groups, catalyst A appears to have deviated from this ordered structure. It is clear

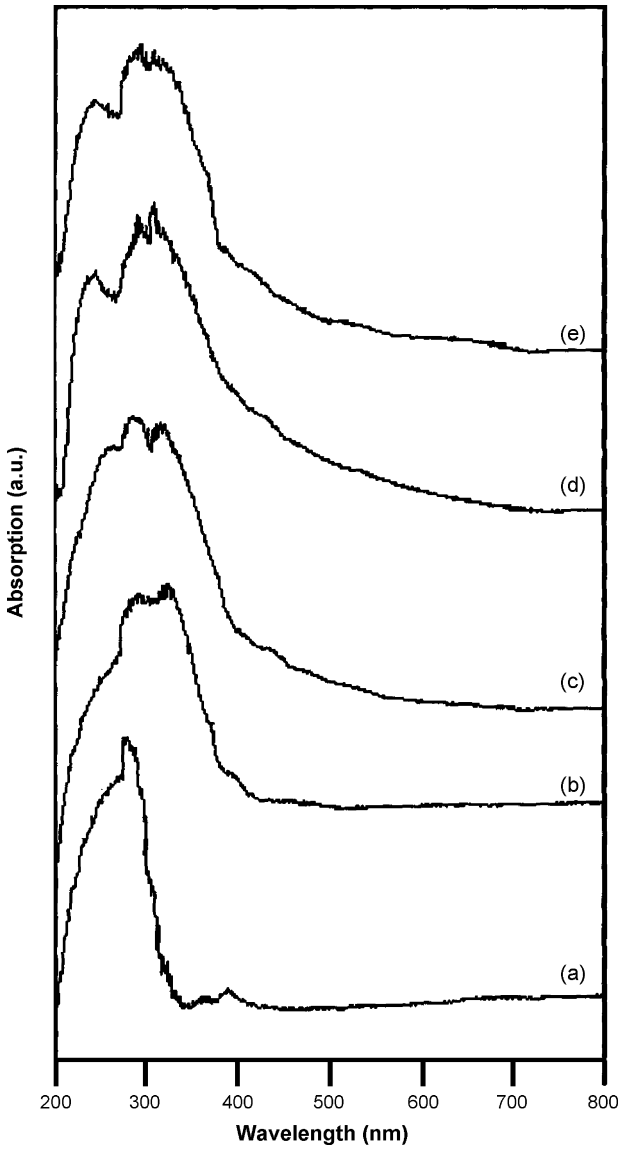

Fig. 3. UV-DRS patterns of (a) catalyst A, (b) catalyst B, (c) catalyst C, (d) catalyst D and (e) catalyst E.

from Raman analysis that the structural changes occurred with the method of preparation.

3.6. TEM studies

Fig. 5 shows the TEM pictures of the $FePO_4$ catalysts. The samples consisted of discrete spherical particles ranging between 30 nm and 200 nm in size, although most of them were between 30 nm and 100 nm. The results are in reasonably good agreement with the crystallite size calculated from the Scherrer equation. Catalyst A showed a kind of agglomeration with cavities and the particles and appeared featureless indicating probably the presence of two different phases, namely the M-phase and the quartz phase. The catalysts, which contained predominantly, quartz structure showed spherical particles with good arrangement. This clearly demonstrates that catalyst A deviated from the morphological structure exhibited

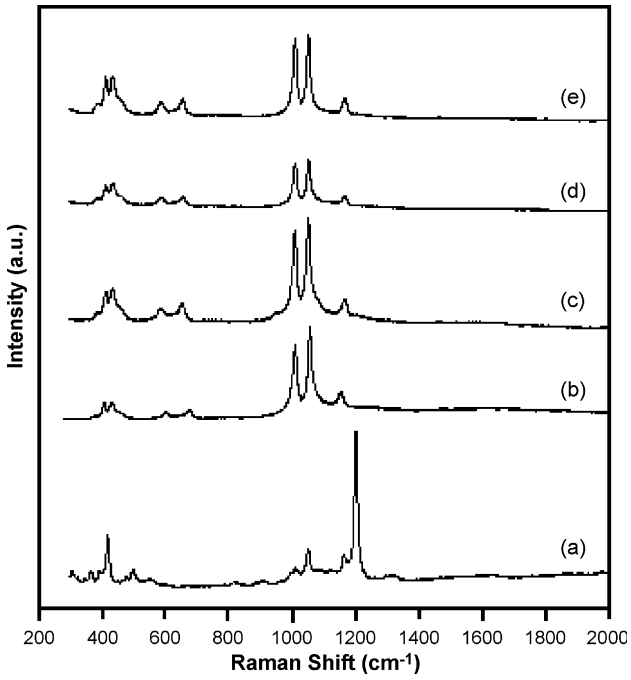

Fig. 4. Laser-Raman spectra of (a) catalyst A, (b) catalyst B, (c) catalyst C, (d) catalyst D and (e) catalyst E.

by other catalysts. This observation is in line with the Raman data.

3.7. Temperature programmed reduction studies

Fig. 6 shows the TPR profiles for the $FePO_4$ catalysts. All these catalysts showed essentially a three-stage reduction behavior except catalyst E, which presented a two-stage reduction phenomenon. It can be seen from Fig. 6 that the positions of the first and third peak were specific to the catalysts from method A to E. The first low temperature H_2 consumption peak is located at 895 K, 843 K, 880 K, 820 K and 885 K, respectively for the five catalysts and the third high temperature peak for the first four catalysts at 1015, 1073, 1010 and 1090 (in catalyst E the third peak merged with the second), respectively. Literature reveals that the stoichiometric catalyst, i.e., with P/Fe = 1.0, shows predominantly one reduction peak at 976 K [17]. Therefore, it is clear that the higher phosphorus content (than the stoichiometric ratio) in the samples induces different structures exhibiting different reduction properties. Following the observations made by Muneyama et al. [6] the first reduction peak is due to reduction of $FePO_4 \rightarrow Fe_3(P_2O_7)_2$. The second peak at 976 K is due to reduction of $Fe_3(P_2O_7)_2 \rightarrow Fe_2P_2O_7$. The third reduction peak can be ascribed to the transformation of $Fe_2P_2O_7 \rightarrow Fe^0$. The second peak, which occurred around 976 K, showed variation in its intensity with method of preparation. It exhibited a maximum intensity in catalyst E wherein the amount of quartz phase formation was also maximum as evidenced by XRD results. Thus the TPR results indicate that the higher the quartz content in the samples, the better is the oxidation state of the Fe stabilized at a value corresponding to $Fe_2P_2O_7$.

3.8. X-ray photo electron spectroscopy studies

The binding energy and the surface P/Fe atomic ratio of each catalyst are summarized in Table 2. The binding energy values for Fe $2p_{3/2}$ and Fe $2p_{1/2}$ of $FePO_4$ catalysts were found to be 712 eV and 727 eV, respectively. These values are in agreement with those reported for Fe^{+3} [17]. This indicates that Fe is present as +3 oxidation state in all the catalysts.

All the $FePO_4$ catalysts showed the binding energy of P 2p at 134.0 eV (Table 2), which corresponds, to the PO_4 group. The binding energy of O 1s for all these catalysts was observed as 530 eV [17]. No noticeable shift was observed with method of preparation. The surface P/Fe ratio, observed by XPS analysis is shown in Table 2. The catalysts showed a surface P/Fe ratio more than the expected value of 1.2 indicating surface enrichment of phosphorous.

3.9. Acidity studies

3.9.1. TPD results

The ammonia desorption peaks observed in between 200 °C and 680 °C for all $FePO_4$ catalysts are shown in Fig. 7. From the literature it is well known that the desorption of ammonia between 180 °C and 250 °C is due to weak acid sites, 250–350 °C due to moderate acid sites and above 350 °C due to strong acid sites present on the surface of the catalysts. Catalyst A showed desorption peaks at two different temperatures i.e. 353 °C and 460 °C indicating that strong acid sites were present on the surface. Catalyst E showed desorption peak of ammonia at 295 °C indicating moderate acid sites. The amount of the total ammonia desorbed per surface area of the iron phosphate catalysts (Table 1) was in the order of catalyst A > B > C > D > E. These observations show that the acidity of catalyst A is stronger as compared with other catalysts. Such results strongly suggest that the acidity property of these catalysts depends on the method of preparation used.

3.9.2. Acidity measurements by potentiometric titration

Fig. 8 shows the potentiometric titration curves of $FePO_4$ catalysts. The acid strength values, expressed as E (mV) are given in Table 1. The acidic strength of surface sites are assigned [15,16] according to the following ranges: very strong site, $E > 100$ mV; strong site, $0 < E < 100$ mV; weak site $-100 < E < 0$ mV and very weak site $E < -100$ mV. It can be seen from the table that very strong acid sites were present on the iron phosphate catalysts. The acid strength of the catalytic samples varied with method of preparation in the order catalyst A > B > C > D > E which is in accordance with the data obtained by TPD of NH_3. It may be noted that this order is reverse to that of quartz phase formation.

3.10. Catalytic functionality of $FePO_4$ catalysts

3.10.1. The ammoxidation activity and its dependence on the method of preparation

The ammoxidation of MP was performed on all the $FePO_4$ catalysts. The main product was CP and the major byproduct

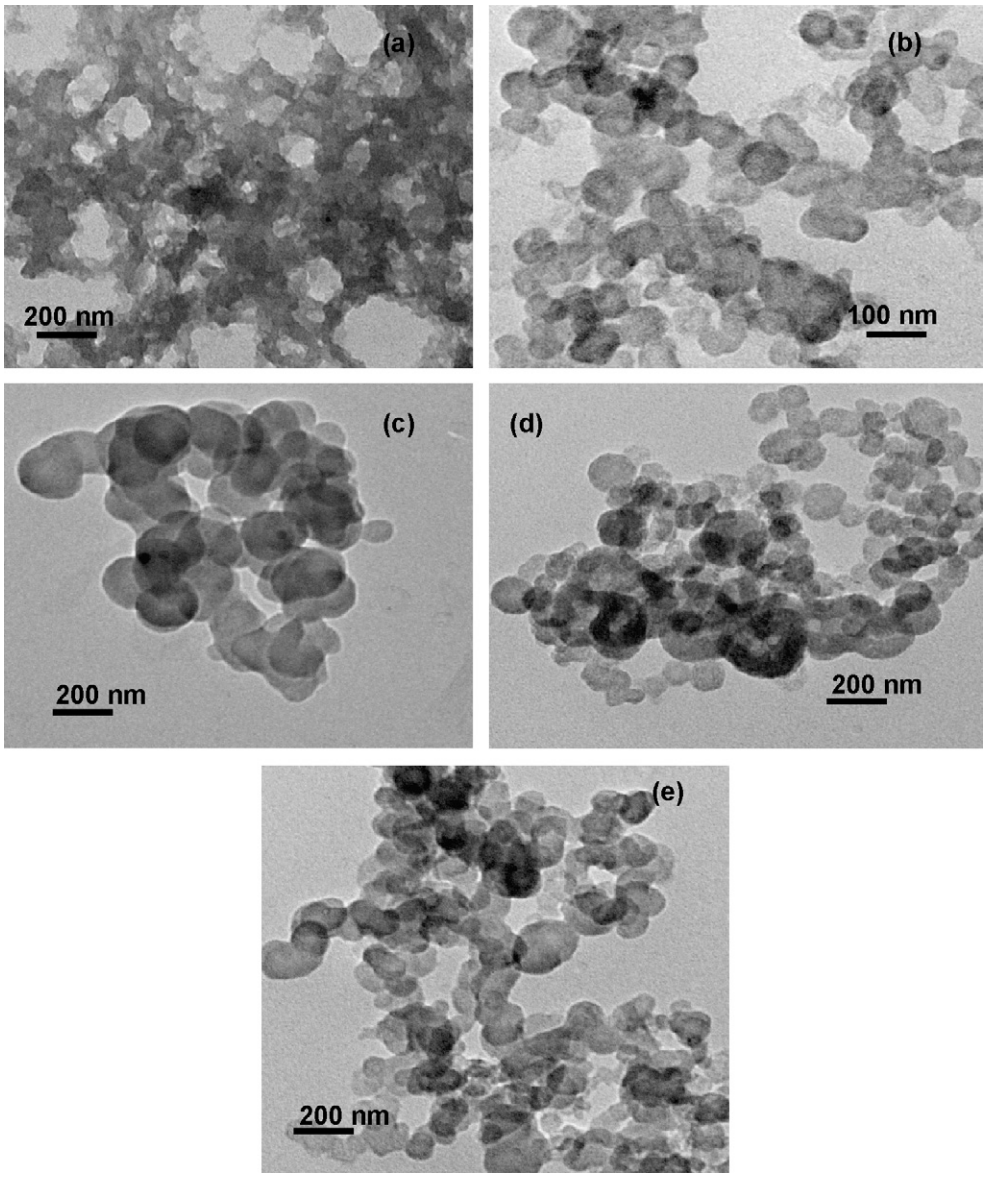

Fig. 5. TEM micrographs of (a) catalyst A, (b) catalyst B, (c) catalyst C, (d) catalyst D and (e) catalyst E.

was pyrazine. Fig. 9(a) displays the variation in the ammoxidation activity (expressed as percent conversion of MP) of the catalysts at different reaction temperatures. Among all the catalysts, catalyst E showed the highest activity. A maximum conversion of 68% was achieved at 693 K. The conversion increased with increase in reaction temperature. The lowest activity was observed in the case of catalyst A where the formation of unknown M-phase was noticed. It seems that the M-phase is inactive for the ammoxidation reaction.

Attention has been focused on the identification of the active phase responsible for the catalytic activity. The XRD patterns (Fig. 1) and UV-Raman (Fig. 4) results clearly indicate that the peaks due to quartz phase were predominant in these catalysts, except in catalyst A. Fig. 9(b) shows a fairly good linear relationship between the extent of quartz phase formation and the conversion, calculated at 653 K. Therefore, it can be presumed that the quartz phase is the active phase whose extent of formation depends on the method of preparation. As the

Table 2
XPS results obtained on the iron phosphate catalysts

Method of preparation	Binding energy (eV) Fe $2p_{3/2}$	Binding energy (eV) P 2p	Binding energy (eV) O 1s	P/Fe atomic ratio
A	712.4	133.8	529.9	2.45
B	712.0	133.6	530.2	2.76
C	711.8	133.7	530.3	2.78
D	711.9	133.5	530.1	2.53
E	712.4	133.8	530.1	1.75

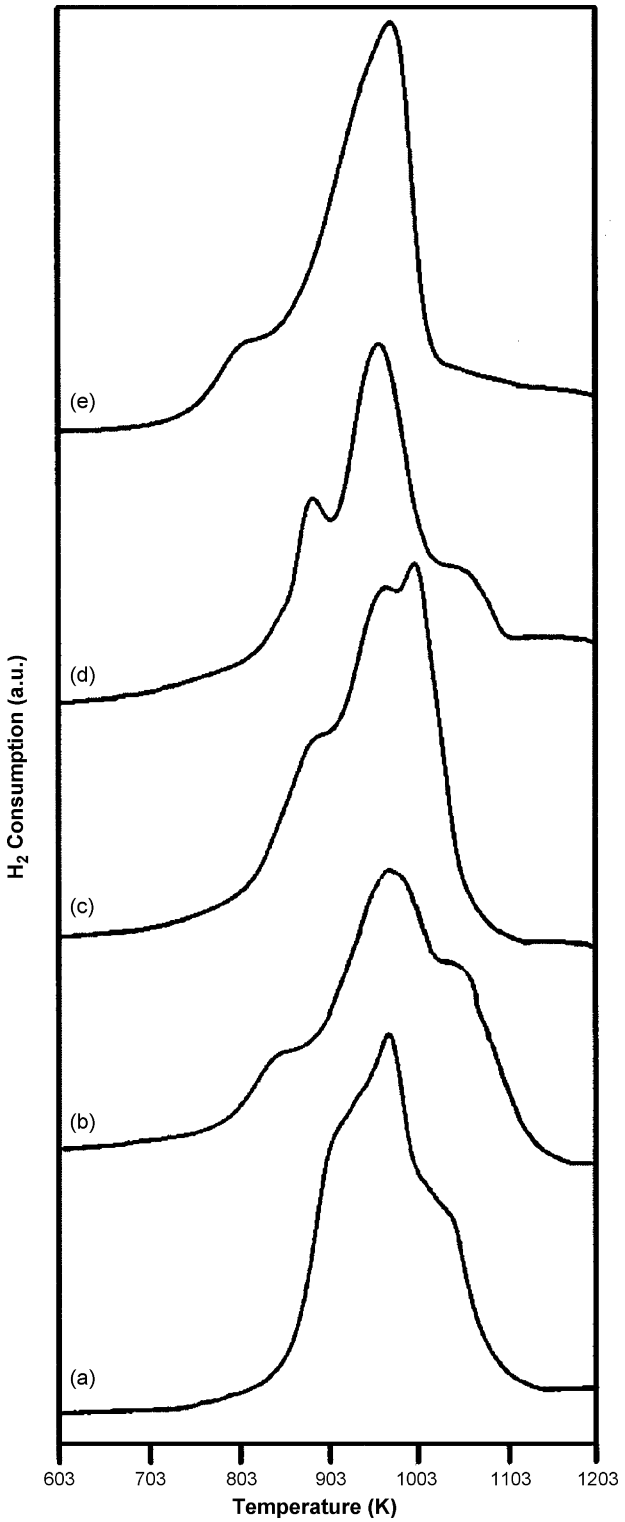

Fig. 6. TPR profiles of (a) catalyst A, (b) catalyst B, (c) catalyst C, (d) catalyst D and (e) catalyst E.

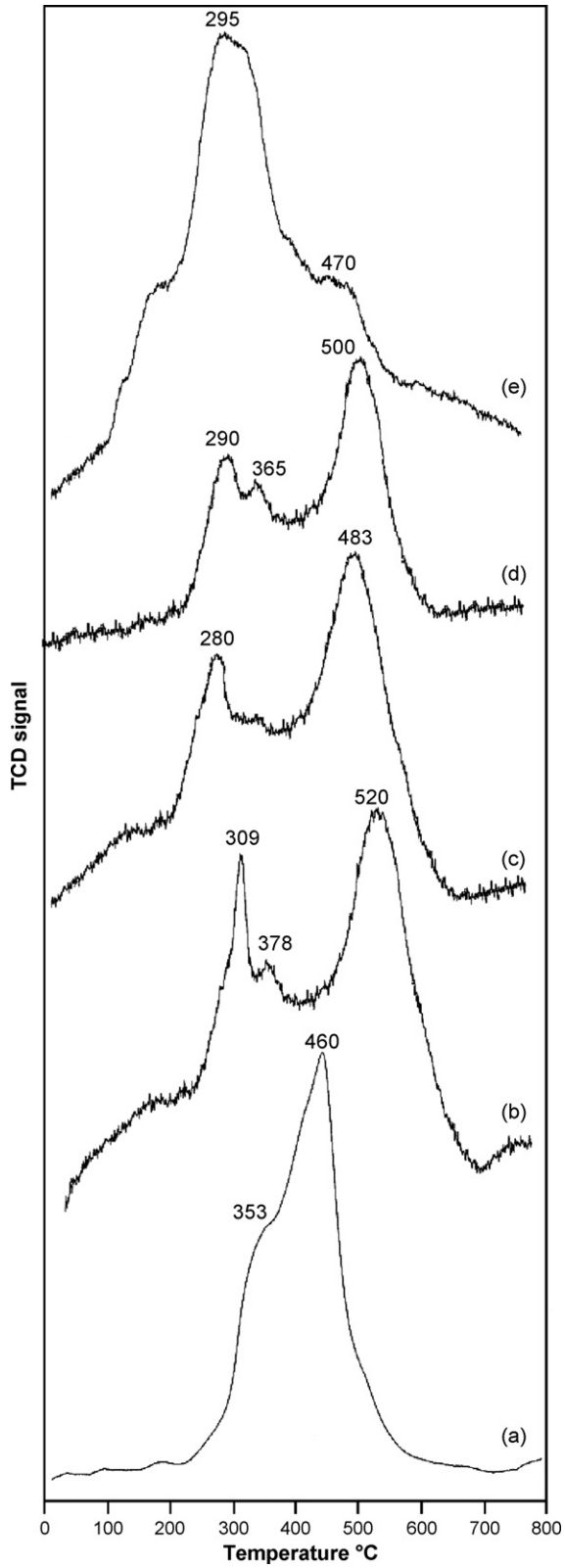

Fig. 7. TPD profiles of (a) catalyst A, (b) catalyst B, (c) catalyst C, (d) catalyst D and (e) catalyst E.

conversion of MP depends on the redox nature of the catalyst, it can be understood that the higher the extent of quartz phase formation, the higher is the redox nature of the catalyst.

The redox nature of iron phosphate catalysts contributing to the conversion of MP was further verified by carrying out the aerobic vapor phase benzyl alcohol oxidation, (as reported by Lingaiah et al. [22]) in a fixed-bed reactor and in the temperature range of 523–583 K. The experimental details are mentioned at the footnote of Fig. 9(c). Benzyl alcohol oxidation leads to two different types of products (i) bezaldehyde (due to

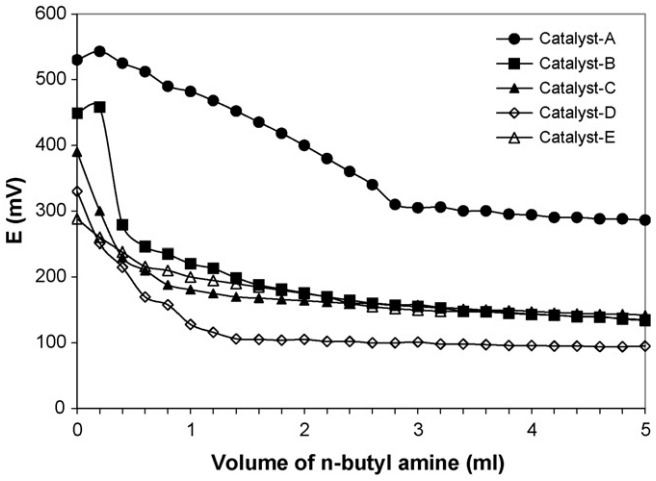

Fig. 8. Potentiometric titration profiles of (a) catalyst A, (b) catalyst B, (c) catalyst C, (d) catalyst D and (e) catalyst E.

redox property of the catalyst) and (ii) dibenzyl ether and toluene (due to acidic property). In the present case, the conversion to benaldehyde is considered for representing the redox property. The maximum oxidation activity to benzaldehyde was shown by catalyst E and the minimum activity was shown by catalyst A (Fig. 9(c)). The conversion increased with increase in reaction temperature. The proportionality between the conversions obtained in ammoxidation and oxidation (Fig. 9(a) and (c)), both representing redox property, is note worthy.

3.10.2. Dependence of selectivity on acidity

The selectivity to CP obtained on various $FePO_4$ catalysts is shown in Fig. 9(d). The selectivity to CP reached a maximum value of 98% on catalyst B at a conversion of nearly 50%, which is the best value for the CP yield obtained. This is the important observation from this work. It was observed that the CP selectivity varied with acid strength of the catalysts. In order to understand how the acid strength affected CP selectivity, the used catalysts were examined by FTIR spectroscopy and the patterns obtained are shown in Fig. 10. The spectra showed IR bands at 1625 cm^{-1}, 2370 cm^{-1}, 1050 cm^{-1}, 920 cm^{-1}, 980 cm^{-1}, 767 cm^{-1} and 511 cm^{-1}. The bands at 1060 cm^{-1}, 980 cm^{-1}, 767 cm^{-1} and 511 cm^{-1} are due to stretching and bending vibrations of the phosphate ion. Catalysts A and B exhibited a peak at 1402 cm^{-1} corresponding to asymmetric stretching mode of the ammonium ion. A considerable decrease in the area of this peak in all other catalytic samples was an interesting observation. It should be noted that the formation of ammonium complex is more facile on catalysts with strong acidity. The high selectivity of the catalysts A and B could be due to the ease of formation of ammonium complex during the course of the reaction because of higher acidity. By pulse

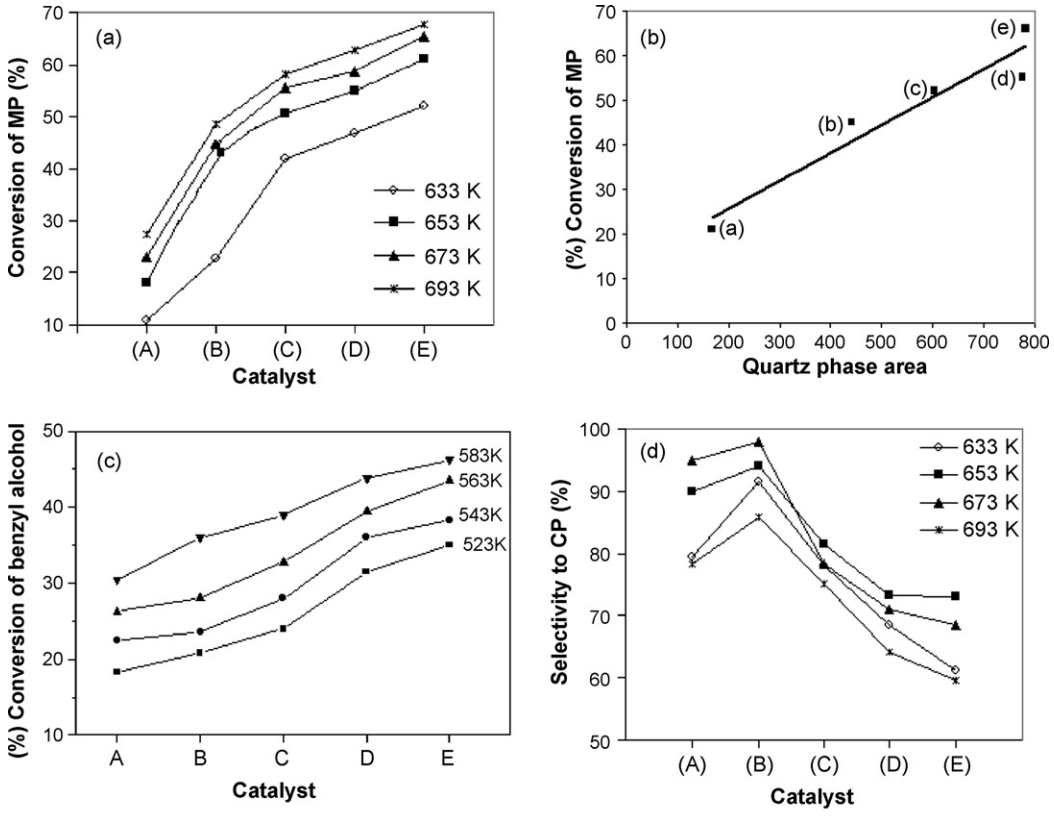

W/F_{liquid} ratio = 0.5 g. cm^{-3}.h, Airflow = 60ml/min.

Fig. 9. (a) Variation of ammoxidation activity at different reaction temperatures. (b) Variation of ammoxidation activity as a function of quartz phase formation in the $FePO_4$ catalysts; (a) catalyst A, (b) catalyst B, (c) catalyst C, (d) catalyst D and (e) catalyst E. (c) Variation of oxidation activity of benzyl alcohol as a function of method of preparation at different reaction temperatures. (d) Variation of ammoxidation selectivity at different reaction temperatures.

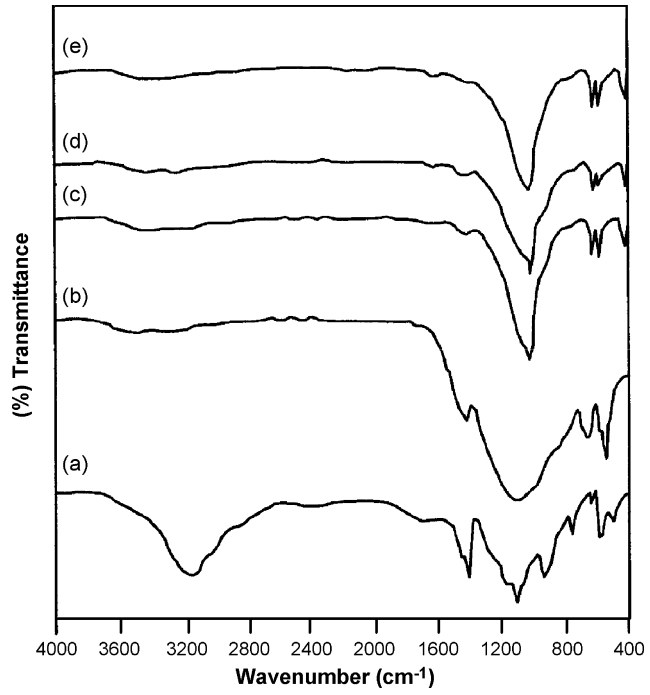

Fig. 10. FTIR spectra of various used iron phosphate (a) catalyst A, (b) catalyst B, (c) catalyst C, (d) catalyst D and (e) catalyst E.

ammoxidation studies, using labeled ammonia, carried out on vanadyl pyrophosphate catalysts, Martin et al. [23] have revealed that the ammonium ion of the complex formed during the reaction reacts with the chemisorbed aldehyde intermediate to form the nitrile. Therefore, it can be thought that the ammonium complex formed predominantly in catalysts A and B might be responsible for higher selectivity.

4. Conclusions

The ammoxidation activity of $FePO_4$ catalysts depends on the extent of quartz phase formation, which in turn is dependent on the nature of preparation. The higher the extent of quartz formation, the higher is the redox nature of the catalysts. The method of catalyst preparation which results in M-phase formation is not suitable for obtaining higher activity. The catalysts prepared in the basic medium loose their acid strength, which leads to reduced nitrile selectivity. In order to obtain better yields of the nitrile product, a judicious combination of the redox and acid properties of the catalysts is required.

Acknowledgements

The authors thank the Director of Indian Institute of Chemical Technology (IICT), Hyderabad, for giving permission to publish these results. Prof. I.E. Wachs of Lehigh University, Bethlehem, USA is acknowledged for providing UV-Raman analysis. The financial assistance of CSIR in the form of a Task Force Project COR-0003 is highly acknowledged.

References

[1] R.G. Rizayev, E.A. Mamedov, V.P. Visloveski, V.E. Sheinin, Appl. Catal. A 83 (1992) 103.
[2] L. Forni, Appl. Catal. 20 (1986) 219.
[3] A. Martin, K.V. Narayana, B. Lücke, J. Sans, Green. Chem. 5 (2002) 481.
[4] A. Martin, B. Lucke, Catal. Today 57 (2000) 61.
[5] S.K. Roy, P. Dutta, L.N. Nandi, S.N. Yadav, T.K. Mondal, S.C. Ray, S. Mitra, P. Samuel, J. Mol. Catal. A 223 (2004) 211.
[6] E. Muneyama, A. Kunishige, K. Ohdhan, M. Ai, J. Catal. 158 (1996) 378.
[7] M. Ai, K. Ohdhan, J. Mol. Catal. A 159 (2000) 19.
[8] M.M. Gadgil, S.K. Kulshreshtha, J. Solid State Chem. 111 (1994) 357.
[9] M. Ai, E. Muneyama, A. Kunishige, K. Ohdan, Appl. Catal. A 109 (1994) 135.
[10] M. Ai, E. Muneyama, A. Kunishige, K. Ohdan, J. Catal. 144 (1993) 632.
[11] M. Ai, K. Ohdan, Appl. Catal. A 165 (1997) 461.
[12] M. Ai, K. Ohdan, Appl. Catal. A 180 (1999) 47.
[13] P. Nagaraju, Ch. Srilakshmi, N. Pasha, N. Lingaiah, I. Suryanarayana, P.S. Sai Prasad, Appl. Catal. A. 334 (2008) 10.
[14] H.P. Klug, L.E. Alexander, X-ray Diffraction Procedures, Wiley, New York, 1954.
[15] P. Villabrille, P. Vazquez, M. Blanco, C. Caceres, J. Colloid Interface 251 (2002) 151.
[16] L.R. Pizzo, P.G. Vazquez, C.V. Caceres, C.V. Blanco, in: Proceedings of the 17th Symposium Iberoam Catal, vol. 1, Porto, Portugal, (July 2000), p. 563.
[17] X. Wang, Y. Wang, Q. Tang, Q. Guo, Q. Zhang, H. Wan, J. Catal. 217 (2003) 457.
[18] P. Bonnet, J.M.M. Millet, C. Leclercq, J.C. Vedrine, J. Catal. 158 (1996) 128.
[19] Q. Yuvan, Q. Zhang, Y. Wang, J. Catal. 233 (2005) 221.
[20] Ch. Srilaxmi, N. Lingaiah, P. Nagaraju, P.S. Sai Prasad, K.V. Narayana, A. Martin, B. Lücke, Appl. Catal. A 309 (2006) 357.
[21] Y. Wang, X. Wang, Z. Su, Q. Guo, Q. Tang, Q. Zhang, H. Wan, Catal. Today 93 (2004) 155.
[22] N. Lingaiah, K. Mohan Reddy, N. Seshu Babu, K. Narasimha Rao, I. Suryanarayana, P.S. Sai Prasad, Cat. Com. 7 (2006) 245.
[23] A. Martin, Y. Zhang, H.W. Zanthoff, M. Meisel, M. Baerns, Appl. Catal. A 139 (1996) 11.